UNICA UNIVERSITÀ DEGLI STUDI DI CAGLIARI

This is the accepted manuscript version of the following contribution:

A. Araújo, O.S.G.P. Soares, C.A. Orge, A.G. Gonçalves, E. Rombi, M.G. Cutrufello, A.M. Fonseca, M.F.R. Pereira, I.C. Neves, **Metal-zeolite catalysts for the removal of pharmaceutical pollutants in water by catalytic ozonation**, *Journal of Environmental Chemical Engineering*, Volume 9, Issue 6, 2021, Article number 106458

The publisher's version is available at:

http://dx.doi.org/ 10.1016/j.jece.2021.106458

When citing, please refer to the published version.

This full text was downloaded from UNICA IRIS https://iris.unica.it/

Metal-zeolite catalysts for the removal of pharmaceutical pollutants in water by catalytic ozonation

A. Araújo,[a] O.S.G.P. Soares,[b] C.A. Orge,[b] A.G. Gonçalves,[b] E. Rombi,[c] M.G. Cutrufello,[c] A.M. Fonseca,[a,d] M.F.R. Pereira[b#] and I.C. Neves[a,d#]

[a.] *CQUM, Chemistry Department, University of Minho, Campus de Gualtar, 4710-057 Braga, Portugal - E-mail: (ineves@quimica.uminho.pt)*

[b.] *Laboratório de Catálise e Materiais (LCM), Laboratório Associado LSRE/LCM, Departamento de Engenharia Química, Faculdade de Engenharia, Universidade do Porto, Rua Dr. Roberto Frias, 4200-465 Porto, Portugal - E-mail: (fpereira@fe.up.pt)*

[c.] *Dipartimento di Scienze Chimiche e Geologiche, Università di Cagliari, Complesso Universitario di Monserrato, S.S. 554 bivio Sestu, 09042 Monserrato, Italy*

[d.] *CEB - Centre of Biological Engineering, Universidade do Minho, Campus Gualtar, 4710-057, Braga, Portugal*

ABSTRACT

Catalytic ozonation of salicylic acid (SA), as model pharmaceutical pollutant, at room temperature was studied in an aqueous phase using mono- (Pd, Cu) and bimetallic (Pd-Cu, Cu-Pd) zeolite catalysts prepared by the ion exchange method, using different zeolite

structures: FAU (USY) and MFI (ZSM5). All metal-zeolite catalysts positively affected SA degradation in comparison with the parent zeolites, except for PdCu-HUSY. The mineralization degree was improved in the presence of the heterogeneous catalysts, regardless of the zeolite used. Nevertheless, the catalysts based on different zeolite structures presented distinct performances during SA oxidation, with those based on HUSY zeolite showing lower activity, which indicated that the physicochemical properties of the zeolite structures are very important. Wide-ranging, the catalytic oxidation of SA with ozone on zeolite-based catalysts was found to be affected by a combination of the acidic properties of zeolites and the chemical composition at the surface. The evolution of oxalic acid as a by-product in SA oxidation, as well as its degradation by catalytic ozonation, were also studied. Reutilization runs revealed that the zeolite-based catalysts were very stable.

KEYWORDS: Catalytic ozonation; Pharmaceutical pollutant; Salicylic acid; CuPd-catalysts; Zeolite structures

1. INTRODUCTION

Conventional water treatment technologies are not effective in degrading pharmaceuticals in wastewater. However, for eliminating traces of these compounds in aquatic environments, advanced oxidation processes have been used. Among these, catalytic ozonation has emerged as a promising water treatment strategy for degrading several priority drinking water contaminants [1,2].

Salicylic acid (SA) is a beta hydroxy acid, chemically classified as monohydroxybenzoic acid, which is commonly used to treat skin disorders, such as comedonal or non-inflamed acne [3], and it has even been shown to reduce the risk of colon cancer [4]. In addition,

SA is the major metabolite and active component of aspirin (acetylsalicylic acid) known for its analgesic, anti-inflammatory, and antipyretic effects [5]. Being an emergent pharmaceutical pollutant, whose concentration has been detected at various levels in the environmental water system, the study of its degradation is a very important issue, also due to the presence of intermediates with a long life-time, such as catechol and oxalic acid, can interfere in its mineralization process [3]. In light of the above, the use of heterogeneous catalysts in the ozonation treatment deserves special attention due to their ability to improve the decomposition of ozone and the formation of hydroxyl radicals, making catalytic ozonation a powerful degradation technology even for refractory compounds [6,7].

Some studies have shown that carbon materials, like activated carbon and multi-walled carbon nanotubes, are efficient ozonation catalysts for removing pharmaceutical pollutants, such as sulfamethoxazole [7], diclofenac [8], nitroimidazole antibiotics [9], and bezafibrate [10].

ZSM5 and NaY zeolites have instead been used to prepare metal-containing catalysts (M = Cu, Pd, Rh, Th, Zn, Ag), which have been successfully employed both in liquid-phase reactions, such as bromate [11,12] and nitrate [13] reduction in water in the presence of hydrogen and in gas-phase reactions, such as ethyl acetate oxidation [14]. Noteworthy, in the case of both MFI (ZSM5) [11] and FAU (NaY) [12-14] structures, the metal-containing catalysts have shown significantly better performance compared to the parent zeolites, with those containing the CuPd pair being the most promising among the investigated catalysts. Moreover, the leaching of the metal components was found to be very low [12], ensuring high stability and reusability of such catalysts.

A remarkable increase in activity after deposition of metals (Pt, Pd, Rh, and Ni) on various oxide supports was also reported for the catalytic ozonation reaction [15]. Catalytic

oxidation with ozone has also been performed to remove VOCs using zeolite as supports or adsorbents [16-18], but only a few works can be found in the literature dealing with zeolites as catalysts for removing pharmaceutical pollutants from water by ozonation. Decomposition of paracetamol in the presence of zeolite A was reported in [19], where the occurrence of a non-radical mechanism, without decomposition of ozone, has been suggested. ZSM5 zeolites with different Si/Al ratios have instead been used in the catalytic ozonation of ibuprofen [20]; it was found that ibuprofen removal is considerably enhanced in the presence of zeolites if compared with ozonation alone and that the adsorption plays a key role in the effectiveness of this process.

This work aimed to develop efficient and stable heterogeneous catalysts to treat pharmaceutical pollutants in water employing catalytic ozonation, using different zeolite structures as supports for metal species. Palladium and copper ions were ion-exchanged on FAU (USY) and MFI (ZSM5) zeolite structures to prepare mono- and bimetallic catalysts. Both the parent zeolites and the metal-containing catalysts were characterized by several techniques and evaluated in the liquid-phase ozonation of salicylic acid at room temperature. These zeolite structures were chosen because they are the most used in catalytic processes and differ in the catalytic proprieties and USY is obtained by steaming of zeolite Y. In addition, degradation of oxalic acid (Oxl), a recalcitrant intermediate, was studied under the same experimental conditions. The reusability of the metal-zeolite catalysts was also investigated.

2. MATERIALS AND METHODS

2.1 Catalysts preparation

Commercial (NH_4)ZSM5 (CBV 3024E) and (NH_4)USY (CBV500) zeolites, provided by Zeolyst International in powder form, were used as supports. The monometallic

catalysts were prepared by the ion-exchange method using palladium ($Pd(NO_3)_2.2H_2O$, Aldrich) or copper ($Cu(NO_3)_2.3H_2O$, Riedel de Haen) nitrates as metal precursors. The detailed preparation procedure is described elsewhere [11,13,14]. The resulting samples were calcined at 500 °C for 4 h under a dry air flow rate of 45 cm^3 min^{-1} and then reduced at 200 °C in hydrogen with a flow rate of 50 cm^3 min^{-1} during 3 h. The obtained samples were named Pd-ZEO and Cu-ZEO (with ZEO = HZSM5 or HUSY). The bimetallic catalysts were prepared by repeating the ion-exchange treatment on the previously synthesized Pd-ZEO and Cu-ZEO samples to obtain CuPd-ZEO and PdCu-ZEO, respectively.

2.2 Characterization methods

Surface area and pore volume were determined from the nitrogen adsorption-desorption isotherms at -196 °C, using a Sorptomatic 1990 System (Fisons Instruments). Before analysis, all samples were outgassed overnight at 250 °C (1 °C min^{-1}) under vacuum. Isotherms were elaborated according to the BET method, applying the treatment suggested by Roquerol et al. [21] for the proper calculation of BET surface area (S_{BET}) of microporous materials. The external surface area (S_{ext}) and micropores volume (V_{micro}) were calculated by the t-plot method. The mesopores volume (V_{meso}) was calculated by the difference between the total pore volume at $P/P_0 = 0.99$ (V_{total}) and V_{micro}.

Inductively coupled plasma atomic emission spectroscopy (ICP-AES) analyses were performed with a 5110 ICP-OES spectrometer (Agilent Technologies). For Na, Al, Si, and Cu determination, ca. 0.015 g of sample were calcined at 500 °C for 12 h, mixed with lithium tetraborate (1:15 w/w), placed in a platinum crucible, and then fused at 1000 °C in a furnace for 30 min. After cooling of the melt, the resultant

fusion bead was dissolved at 80 °C for about 30 min with 20 mL of a HNO_3 solution (0.80 M) and finally diluted to the desired volume by Milli-Q water. Pd content was determined by treating the solid (ca. 0.015 g) with a mixture of HCl (37%) and HNO_3 (70%) (3:1 by volume) at 80 °C for 3 h to dissolve Pd. The suspension was then filtered, the filtrate recovered, and finally diluted to the desired volume by Milli-Q water.

Scanning electron micrographs (SEM) of the catalysts were collected on a Jeol JSM-6010LV Scanning Microscope equipped with an EDX system. In order to avoid surface charging, the samples were previously placed in carbon tape and coated with a thin layer of gold (5 nm) for 15 min at a pressure of 5-10 Torr by using a Polaron SC502 sputter coater. The magnification of 5000x and 15000x were used with an energy beam of 15 kV.

X-ray photoelectron spectroscopy (XPS) was performed at Centro de Apoyo Científico y Tecnologíco a la Investigación (C.A.C.T.I.), University of Vigo, Spain. Analysis of the samples was performed using a TermoScientific K-Alpha ESCA instrument, equipped with aluminium Kα monochromatized radiation at 1486.6 eV X-ray source. Due to the non-conducting nature of the samples, an electron flood gun was used to minimize surface charging. Neutralization of the surface charge was performed by using both a low energy flood gun (electrons in the range 0 to 14 eV) and a low energy Argon ions gun. Photoelectrons were collected from a take-off angle of 90^0 relative to the sample surface. The measurement was done in a Constant Analyser Energy mode (CAE) with a 100 eV pass energy for survey spectra and 20 eV pass energy for high-resolution spectra. Surface elemental composition was determined using the standard Scofield photoemission cross sections.

Temperature Programmed Reduction (TPR) analyses were performed on a TPD/R/O 1100 instrument (Thermoquest) equipped with a TCD detector. H_2 (5%vol in N_2) was used as the reducing agent. About 0.1 g of sample was put in contact with the gaseous mixture (30 cm^3 min^{-1}) in the temperature range 50-600 °C (heating rate, 5 °C min^{-1}). Prior to analysis, samples were thermally treated under air flow (20 cm^3 min^{-1}) at 500 °C (heating rate, 10 °C min^{-1}) for 2 h and then cooled to 50 °C in flowing N_2 (20 cm^3 min^{-1}).

Thermogravimetric analyses (TG) of the samples were carried out on a Perkin-Elmer STA6000 thermal analyzer, heating under nitrogen flow (20 cm^3 min^{-1}) from 25 to 800 °C (heating rate of 10 °C min^{-1}). Prior to analysis, the samples were equilibrated with water vapor at ambient temperature for 18 h.

Microcalorimetric analysis was performed on a Tian-Calvet heat flow calorimeter (Setaram) equipped with a volumetric vacuum line. About 0.1 g of sample were pretreated overnight at 250 °C under vacuum ($7.5x10^{-6}$ Torr) prior to analysis. Small doses of the probe gas (NH_3) were successively introduced into the measuring cell, the equilibrium pressure relative to each adsorbed amount was measured by means of a differential pressure gauge (Datametrics), and the thermal effect was recorded. The experiment was performed at 80 °C (in order to limit physisorption) up to a final equilibrium pressure of ca. 1 Torr. After overnight outgassing, a second adsorption run was carried out in the same conditions to estimate the extent of irreversible adsorption.

2.3 Catalytic tests

Ozonation tests were performed at room temperature (25 °C) in a laboratory-scale reactor (1 L), equipped with a magnetic stirrer (300 rpm) and a circulation jacket.

Salicylic acid (SA) was chosen as the model molecule for emergent pharmaceutical pollutants in water. For each test, the reactor was filled with 700 mL of a SA solution (0.5 mM) and 350 mg of catalyst. Ozone feeding gas was produced from pure oxygen in a BMT 802X generator, and it was monitored with a BMT 964 ozone analyzer. The total inlet flow rate was 150 cm^3 min^{-1}, with an O_3 concentration of 50 g m^{-3} (0.05 mg cm^{-3}). Unreacted ozone at the reactor outlet was treated in a solution of potassium iodide (KI). Liquid-phase was sampled at specific times and analyzed with HPLC to follow the SA concentration in solution and to verify the presence of recalcitrant intermediates. Degradation of oxalic acid was also investigated using the same conditions. The initial pH values were 3.4 and 3.0 for SA and oxalic acid, respectively. In the case of SA oxidation, the stability of the catalysts was studied by performing recycling experiments in the same experimental conditions as above. Five runs were performed, each lasting 5 h. After each run, the catalyst was dried in an oven at 100 ^oC overnight before reutilization. Catalytic tests were performed in duplicate, and the maximum deviation observed in the removal of the organic pollutant was 2%. The amounts of metals eventually leached during the reaction were measured in a UNICAM 939/959 atomic absorption spectrometer (AAS), using the remaining solution after selected reaction tests.

3 RESULTS AND DISCUSSION

3.1 Characterization of metal-ZEO catalysts

Results of the textural analysis are shown in Fig. S1 (see Supplementary Material). All samples present a Type I isotherm, typical of microporous materials. Narrow hysteresis loops are visible at high P/P_0 values, more easily identifiable in the case of the HUSY-based series, which can be ascribed to the presence of mesoporosity

originating from interparticle voids. The textural properties of the parent zeolites and the metal-ZEO catalysts obtained by nitrogen physisorption are displayed in Table 1.

Table 1. Textural properties of the parent zeolite and the samples.

Samples	S_{BET}[a] (m^2/g)	V_{total}[b] (cm^3/g)	S_{ext}[c] (m^2/g)	V_{micro}[c] (cm^3/g)	V_{meso}[d] (cm^3/g)
HUSY	682	0.32	164	0.20	0.12
Pd-HUSY	710	0.33	164	0.21	0.12
Cu-HUSY	728	0.36	198	0.21	0.15
PdCu-HUSY	665	0.32	168	0.19	0.13
CuPd-HUSY	652	0.35	203	0.18	0.17
HZSM5	411	0.26	169	0.10	0.16
Pd-HZSM5	432	0.26	177	0.10	0.16
Cu-HZSM5	448	0.26	225	0.10	0.16
PdCu-HZSM5	407	0.27	150	0.10	0.17
CuPd-HZSM5	418	0.26	156	0.11	0.15

[a]Surface area calculated from the BET equation according to [21];
[b]Total pore volume determined from the amount adsorbed at $P/P_0 = 0.99$;
[c]External surface area and micropores volume calculated by the t-method;
[d]Mesopores volume calculated by the difference V_{total}-V_{micro}.

Compared to the parent HUSY zeolite, a slightly increase in the specific surface area is observed for the Pd-HUSY and Cu-HUSY. Such increase could be due to slight changes in the porous structure triggered by the ion exchange treatment, most likely during the calcination step at 500 °C. In the case of Cu-HUSY, an increase in external surface area and mesoporous volume is also observed. For the bimetallic catalysts, a

diminution in both S_{BET} and V_{micro} values below those of the parent zeolite occurs after the addition of the second metal, suggesting that the insertion of the metal could partially obstruct the micropores. By converse, compared to both the parent structures and the corresponding monometallic catalysts, a rise in S_{ext} and V_{meso} can be noted for PdCu-HUSY and CuPd-HUSY, although being very slight in the case of the former sample.

Concerning the catalysts based on HZSM5, the Pd-HZSM5 and Cu-HZSM5 samples show increased S_{BET} and S_{ext} values compared to the parent zeolite, while no changes are observed for the other parameters. Similar to the case of the HUSY-based catalysts, the total surface area diminishes after the addition of the second metal; however, at variance with that system, a decrease in the external surface area is also observed.

By comparing the two catalysts series, it emerges that all the samples in the HUSY series have higher values of both S_{BET} and V_{total}, in agreement with the results reported in [18] for Ru-Mn/HZSM-5 and Ru-Mn/HY catalysts. Compared to the HZSM5-based ones, the HUSY-based catalysts also show almost doubled V_{micro} values, whereas the mesoporous volume is slightly lower except for the CuPd-HUSY.

ICP-AES analysis was performed on the protonic form of the parent zeolites to determine the Si/Al molar ratio. Values of 3.00 and 15.0 for the Si/Al molar ratio were estimated for HUSY and HZSM5, respectively. Determination of the pH_{pzc} was also carried out according to the procedure reported in [11]. Comparable values were obtained for the two parent zeolites (4.5 and 4.4 for HUSY and HZSM5, respectively), which confirms their acidic properties due to the presence of protons in their framework as a consequence of NH_4^+ decomposition into H^+ and NH_3 during

the calcination step. Pd and Cu amounts, also quantified by ICP-AES, are reported in Table 2.

Table 2. Palladium and copper contents determined by ICP-AES and by EDX elemental analysis.

Samples	Pd (wt%)		Cu (wt%)		Pd/Cu (atomic ratio)	
	ICP-AES	EDX	ICP-AES	EDX	ICP-AES	EDX
Pd-HUSY	1.47	n.d.	-	-	-	-
Cu-HUSY	-	-	1.04	n.d.	-	-
PdCu-HUSY	1.45	1.80	0.63	0.70	1.39	1.54
CuPd-HUSY	1.11	1.70	0.49	0.40	1.35	2.54
Pd-HZSM5	1.08	n.d.	-	-	-	
Cu-HZSM5	-	-	0.56	n.d.	-	
PdCu-HZSM5	1.76	1.50	0.33	0.40	3.22	2.24
CuPd-HZSM5	1.03	1.10	0.50	0.70	1.20	0.94

[n.d]not determined

Both zeolite structures showed has affinity for these divalent cations. Concerning the monometallic samples, a higher metal loading is observed for the Pd- and Cu-HUSY catalysts, which might be ascribed to the higher cation-exchange capacity of such zeolite compared to HZSM5, due to its significantly higher Al content. However, in the case of the bimetallic catalysts, the total metal loading does not seem to depend on the zeolite structure, being similar for the two PdCu- and CuPd-ZEO series. By taking into account that the introduction of the second metal is performed on the

calcined monometallic catalyst (i.e. on the protonic form of the support), this could be justified by the lower tendency of the protons to be exchanged compared to the ammonium ions.

The calculated noble metal/copper atomic ratios are practically the same for the two HUSY-based samples (1.39 and 1.35 for PdCu-HUSY and CuPd-HUSY, respectively), while they are significantly different in the case of the HZSM5-supported catalysts, being 3.22 and 1.20 for PdCu-HZSM5 and CuPd-HZSM5, respectively.

SEM micrographs and EDX elemental analyses of the CuPd-HUSY and CuPd-HZSM5 samples, chosen as representatives of the two catalysts series, are shown in Fig. 1. SEM analysis demonstrates that the typical morphology of the parent zeolites is preserved in all the metal-containing catalysts, indicating that the ion-exchange treatment does not induce any significant modification. EDX analysis of the bimetallic samples confirms the presence of both Pd and Cu species, whose amounts are reported in Table 2. The differences between the palladium and copper contents quantified by EDX and by ICP-AES suggest a certain degree of inhomogeneity in the concentration profiles through the support, despite the use of the ion-exchange treatment, which would guarantee a homogeneous deposition of the metals [22-24].

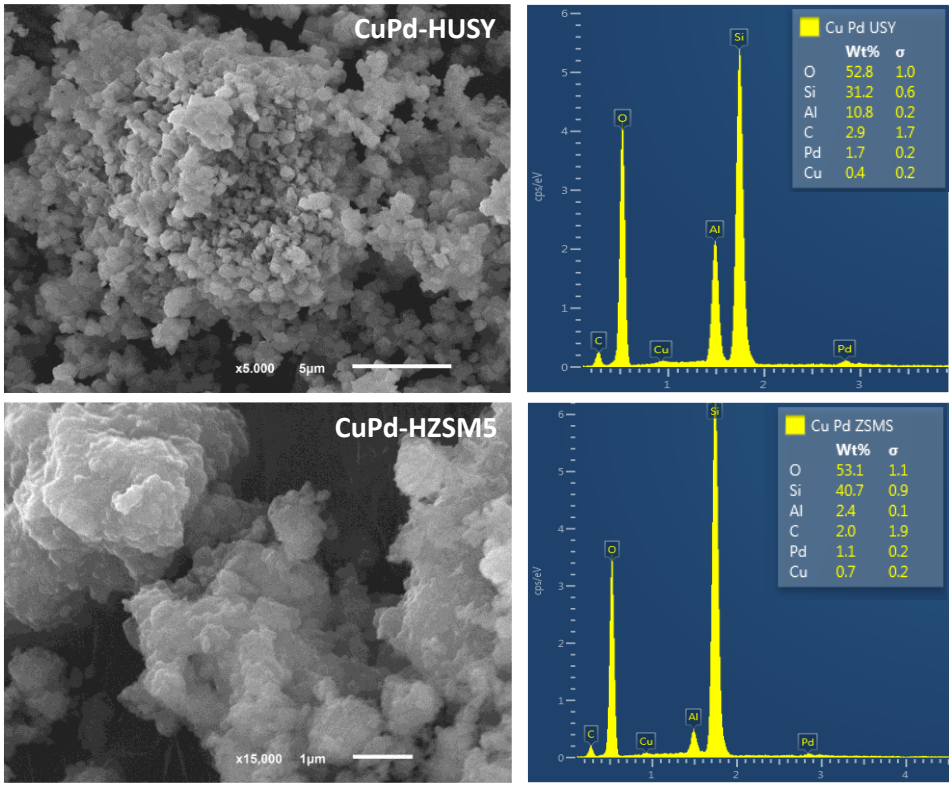

Fig. 1 SEM images of CuPd-HUSY and CuPd-HZSM5 with different resolutions and their EDX spectra.

The bimetallic-ZEO samples were analysed by XPS. Besides the typical zeolite elements, i.e. oxygen, sodium, silicon, and aluminum, copper and palladium species were also detected in the survey XPS resolution spectrum of the samples (Fig. S2, see Supplementary Material). The existence of both the metallic and ionic forms of the two species can be inferred by closely inspecting the signals in the Cu 2p and Pd 3d binding energy (BE) ranges in the high-resolution spectra. As an example, the XPS high-resolution spectra of the Cu 2p and Pd 3d regions of the bimetallic-HUSY samples are displayed in Fig. 2.

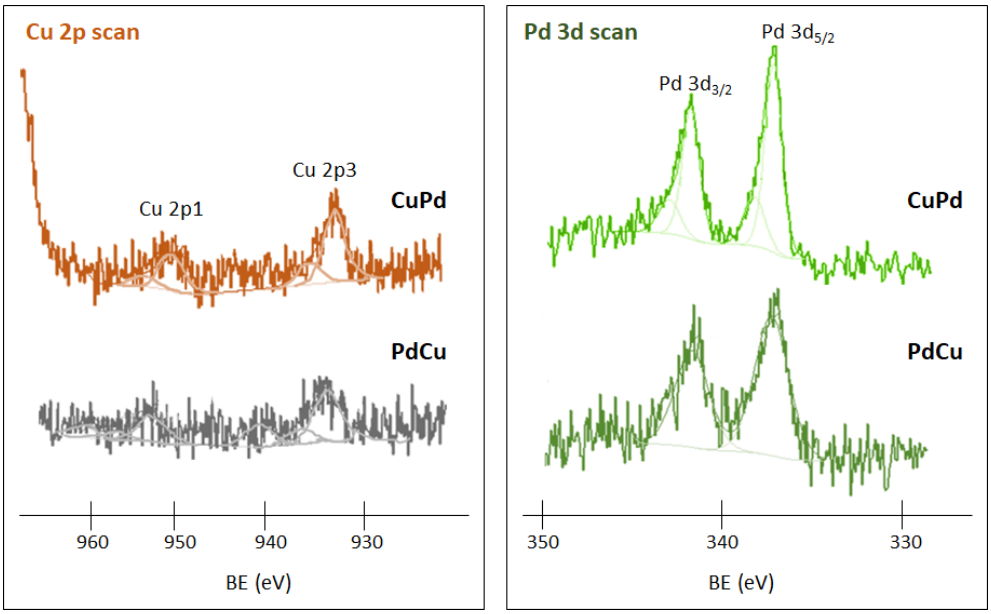

Fig. 2. XPS high-resolution spectra of the Cu 2p and Pd 3d regions of the bimetallic-HUSY samples.

XPS results for all the prepared bimetallic samples are summarized in Tables 3 and 4, where the Cu 2p and Pd 3d binding energy values, the surface composition, the copper and palladium oxidation states, and the relative amount of M(0) and M(II) species (M = Pd, Cu) are reported.

Table 3. Pd and Cu species in XPS spectra of the bimetallic-ZEO samples. Identification of binding energy (BE), the atomic percentage of the metals on the surface of the different oxidation states.

Samples	Survey XPS spectra in the Cu 2p and Pd 3d regions				High resolution XPS spectra in the Cu 2p and Pd 3d regions	
	Cu 2p (BE)	Pd 3d (BE)	M (at%)	Pd/Cu	Cu 2p (BE)	Pd 3d (BE)
PdCu-HUSY	933.6	336.3	0.29 (Pd) 0.34 (Cu)	0.85	933.3/Cu(0) 936.2/Cu(II)	335.8/Pd(0) 337.9/Pd(II)

CuPd-HUSY	933.2	336.2	0.37 (Pd) 0.34 (Cu)	1.09	932.5/Cu(0) 935.8/Cu(II)	335.9/Pd(0) 337.1/Pd(II)
PdCu-HZSM5	933.7	336.3	0.17 (Pd) 0.15 (Cu)	1.39	933.6/Cu(0) 935.7/Cu(II)	335.7/Pd(0) 337.8/Pd(II)
CuPd-HZSM5	933.2	336.4	0.25 (Pd) 0.18 (Cu)	1.13	933.5/Cu(0) 936.1/Cu(II)	335.2/Pd(0) 337.7/Pd(II)

The Cu $2p_{3/2}$ and $2p_{1/2}$ signals are observed in the range 930 to 960 eV and consist of two contributions, indicating the presence of copper in different oxidation states. In particular, for Cu $2p_{3/2}$, such contributions are centered at 933 and 936 eV and can be ascribed to Cu(0) and Cu(II), respectively [25-28]. The Pd 3d signals are observed in the BE ranges 334-338 ($3d_{5/2}$) and 339-344 ($3d_{3/2}$) eV. Each component of the doublet can be fitted by two contributions, ascribable to Pd in different oxidation states.

According to the literature, Pd(0) is responsible for the signals at ca. 335 and 340 eV [27,29], while the peaks at ca. 337 and 341.5 eV are indicative of the presence of Pd^{2+} species [30-32]. The obtained results highlight that a fraction of the original Cu^{2+} and Pd^{2+} is not completely transformed into metallic form after the reduction pre-treatment at 200 °C, most probably due to the occurrence of strong interactions with the zeolite structure. In the bimetallic catalysts, the slight shift of BE in the Cu 2p and Pd 3d regions observed between FAU and MFI structures are due to the differences in the physicochemical properties of the zeolites and also to the order of the introduction of the metal ions after the treatments. The presence of the M(II)/M(0) couple was also demonstrated by cyclic voltammetry studies in the case of NaY-supported CuPd and PdCu bimetallic catalysts [13].

Table 4. Pd and Cu species in XPS spectra of the bimetallic-ZEO samples. Identification and contribution on the surface of the different oxidation states.

Samples	Contribution of different oxidation states of Cu 2p and Pd 3d regions from high resolution XPS spectra			
	Cu 2p (%)	Cu(0)/Cu(II)	Pd 3d (%)	Pd(0)/Pd(II)
PdCu-HUSY	Cu(0) - 57 Cu(II) - 43	1.3	Pd(0) - 59 Pd(II) - 41	1.4
CuPd-HUSY	Cu(0) - 86 Cu(II) - 14	6.1	Pd(0) - 76 Pd(II) - 24	3.2
PdCu-HZSM5	Cu(0) - 53 Cu(II) - 47	1.1	Pd(0) - 75 Pd(II) - 25	3.0
CuPd-HZSM5	Cu(0) - 67 Cu(II) - 33	2.0	Pd(0) - 81 Pd(II) - 19	4.3

Notably, by comparing the surface Pd/Cu atomic ratio (Table 3) with the bulk value determined by chemical analysis (Table 2), it emerges that the former is lower, confirming a heterogeneous distribution of the metals throughout the bimetallic samples. For the PdCu-ZEO catalysts, the surface Pd/Cu atomic ratio is much smaller than the bulk ratio: 0.85 (XPS) and 1.39 (ICP) for PdCu-HUSY catalysts, 1.39 (XPS) and 3.22 (ICP) for PdCu-HZSM5 catalysts, indicating a surface enrichment of Cu. However, when the second metal added is palladium, the Pd/Cu atomic ratios are more similar: 1.09 (XPS) and 1.35 (ICP) for CuPd-HUSY catalysts, 1.13 (XPS) and 1.20 (ICP) for CuPd-HZSM5 catalysts. Moreover, the Pd(0)/Pd(II) and Cu(0)/Cu(II) ratios in the bimetallic catalysts (Table 4) are different and depend on the zeolite

structure, the Pd(0)/Pd(II) ratio being lower for the bimetallic-HUSY catalysts, while the opposite is true for the Cu(0)/Cu(II) ratio.

H_2-TPR profiles of the mono- and bimetallic catalysts are reported in Fig. 3 for the HUSY- (Fig. 3A) and HZSM5-based (Fig. 3B) catalysts. TPR curves of the parent zeolites are also reported for comparison, both showing a peak around 250 °C, which could probably be ascribed to the reduction of impurities. As well known, differences in both the profile shape and the temperature of maximum H_2 consumption, apart from the nature of the reducible species and the support, also depend on the adopted experimental conditions.

By looking at Fig. 3A, a very broad contribution is observable for Cu-HUSY between 150 and 550 °C (curve b), with a maximum at ca. 350 °C. Reduction peaks in the range 250-320 °C were observed by several authors for Cu supported on γ-alumina [33,34], NaY [35] and H-mordenite [35].

However, noticeably higher H_2-consumption temperatures were reported in [36] for a Cu/Al_2O_3 catalyst, whose TPR profile showed two broad peaks centered at 370 and 468 °C. The first peak was ascribed to the presence of highly dispersed reducible Cu^{2+} species, in the form of isolated copper ions and/or two- and three-dimensional copper oxide clusters, while the second one was assigned to the reduction of Cu^{+} species (deriving from the partial reduction of the original Cu^{2+} types) to Cu^{0}. According to the literature, the high-temperature contribution in the TPR profile of the Cu-HUSY sample may hence be attributed to the presence of Cu^{2+} species with a high dispersion on the support. The Pd-HUSY sample shows a well-defined peak at about 120 °C, which can be ascribed to the reduction of Pd oxide species strongly interacting with the support [37,38]. However, the presence of PdO_x clusters, which were found to reduce below 50 °C [37,38], cannot be ruled out because of the adopted

experimental conditions (TPR starting temperature = 50 °C). By closely inspecting curve c in Fig. 3A, a small negative peak seems to appear at about 55 °C that, according to [34,36-38], originates by decomposition of Pd β-hydrides (formed on Pd^0 deriving from the reduction of PdO_x clusters). However, the very low intensity of such peak, though suggesting the existence of PdO_x clusters, hints at their presence in little amounts and/or small sizes.

In the case of the CuPd-HUSY (curve d), a small negative peak at ca. 60 °C is still identifiable (indicating the presence of a few PdO_x clusters in the starting material), while it is not observable in the profile of PdCu-HUSY (curve e). For both the bimetallic catalysts, the peak originally centered at ca. 120 °C moves above 135 °C and appears enlarged compared to that of Pd-HUSY. Instead, no contributions are clearly visible in the temperature range of Cu^{2+} reduction on Cu-HUSY. The presence of a single peak, as well as its displacement at different temperatures compared to the corresponding monometallic samples, was already reported for Al_2O_3-supported [33] and NaY-supported [13] Pd-Cu catalysts. In agreement with the literature, it can be proposed that, for the present bimetallic HUSY-based catalysts, changes observed in both the shape and maximum temperature of the H_2-consumption peak can to a large extent be ascribed to the presence of Pd^{2+} and Cu^{2+} reducible species in close interaction, where Pd^0 previously forms and promotes Cu^{2+} reduction [33].

Concerning the HZSM5-based catalysts (Fig. 3B), a broad contribution still appears in the TPR profile of the Cu-HZSM5 (curve b), located at temperatures between 300 and 600 °C, i.e. higher than those of Cu-HUSY, which suggests the existence of less reducible Cu^{2+} species. Interestingly, apart from the peak ascribed to the parent zeolite and centered at 250 °C, two more peaks are visible in the case of the Pd-HZSM5 (curve c), the former at about 100 °C, which seems to be preceded by a

negative signal of low intensity, ascribable to the decomposition of a small amount of Pd β-hydrides, and the latter above 400 °C. As in the case of the Pd-HUSY, the low-temperature contribution can be related to the reduction of Pd oxides species with strong interactions with the support. Instead, according to [39], the peak centered at 435 °C might be ascribed to the reduction of Pd oxides species in ion-exchanged positions where Pd^{2+} ions are stabilized largely by the higher negative charge density. For the bimetallic catalysts (Fig. 3B), a shift of the maximum of the low-temperature Pd-reduction peak towards higher temperatures is observed for both CuPd-HZSM5 (curve d) and PdCu-HZSM5 (curve e), the latter also showing a small negative contribution related to the Pd β-hydrides decomposition.

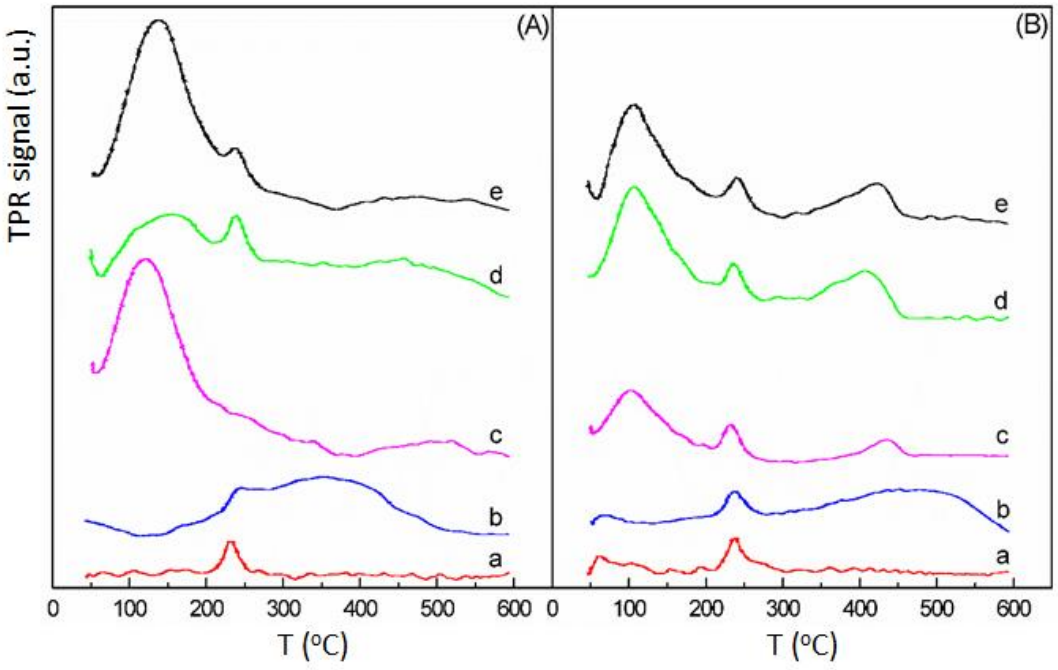

Fig. 3 H_2-TPR profiles of the mono- and bimetallic catalysts of (A) HUSY-based (B) and HZSM5-based: (a) parent zeolite; (b) Cu-ZEO; (c) Pd-ZEO; (d) CuPd-ZEO and (e) PdCu-ZEO.

As previously mentioned, the observed increase in the temperature of maximum hydrogen consumption is indicative of interactions between the two metal components. It is worthy of note that, in the case of the bimetallic HZSM5-based catalysts, reduction peaks are clearly visible between 330 and 460 °C, with maxima at 410 and 425 °C for CuPd-HZSM5 and PdCu-HZSM5, respectively. The intensity of such peaks, being markedly higher than that of Pd-HZSM5, clearly indicates that, besides Pd^{2+} ions, Cu^{2+} species would contribute to the H_2 consumption. This highlights the close interaction of Cu^{2+} species with both types of Pd^{2+} species, which is responsible for the enhanced mutual reducibility of the two metal components. The presence of different metal species is in agreement with XPS analysis.

Results of the thermogravimetric analysis are reported in Fig. S3 and summarized in Table S1 (see Supplementary Material). The weight loss between 25 and 200 °C, which is related to water release, is in the range 17 - 21% and 9 - 11% for the HUSY and HZSM5 series, respectively, and is only slightly affected by the presence of the metals. In comparison with HUSY and the corresponding metal-containing catalysts, the much lower amount of water adsorbed on the HZSM5-based catalysts indicates their higher hydrophobicity, as also confirmed by the fact that for such samples, more than 80% of the water is released below 110 °C (Fig. S3). The hydrophobicity of the HZSM5-based catalysts could influence the reaction, as it could favour the adsorption of the SA molecules on the acid sites.

The acidic properties of the samples were investigated by microcalorimetry, and the results are summarized in Fig. 4. For all the samples, trends of the differential adsorption heat (Q_{diff}) are shown as a function of NH_3 uptake (Fig. 4A and 4B) to obtain information on the influence of the surface coverage on the energetics of the adsorption on acid sites (n_A). The cut-off value between chemisorption and

physisorption (the latter corresponding to Q_{diff} as low as 2-3 times the condensation heat of the probe molecule [40]) was fixed at 60 kJ mol^{-1}, being the heat of NH_3 condensation at 80 °C equal to 20.2 kJ mol^{-1} [40].

As for the HUSY-based catalysts, upon adsorption of the initial dose of NH_3, high Q_{diff} values are observed in the range 180-230 kJ mol^{-1} (Fig. 4A), indicative of the presence of small amounts of very strong acid sites. After a sharp decrease at very low coverages, the Q_{diff} profiles show, for all the samples, a step in the range 115-135 kJ mol^{-1}, before continuing to decrease until reaching the non-specific adsorption region. Such steps indicate the existence of families of energetically homogeneous sites and can be better identified from the acid site energy distribution plots, $-dn_A/dQ_{diff}$ vs. Q_{diff}, obtainable from the Q_{diff} vs. NH_3 coverage curves, which can be regarded as the acid strength spectra of the catalysts.

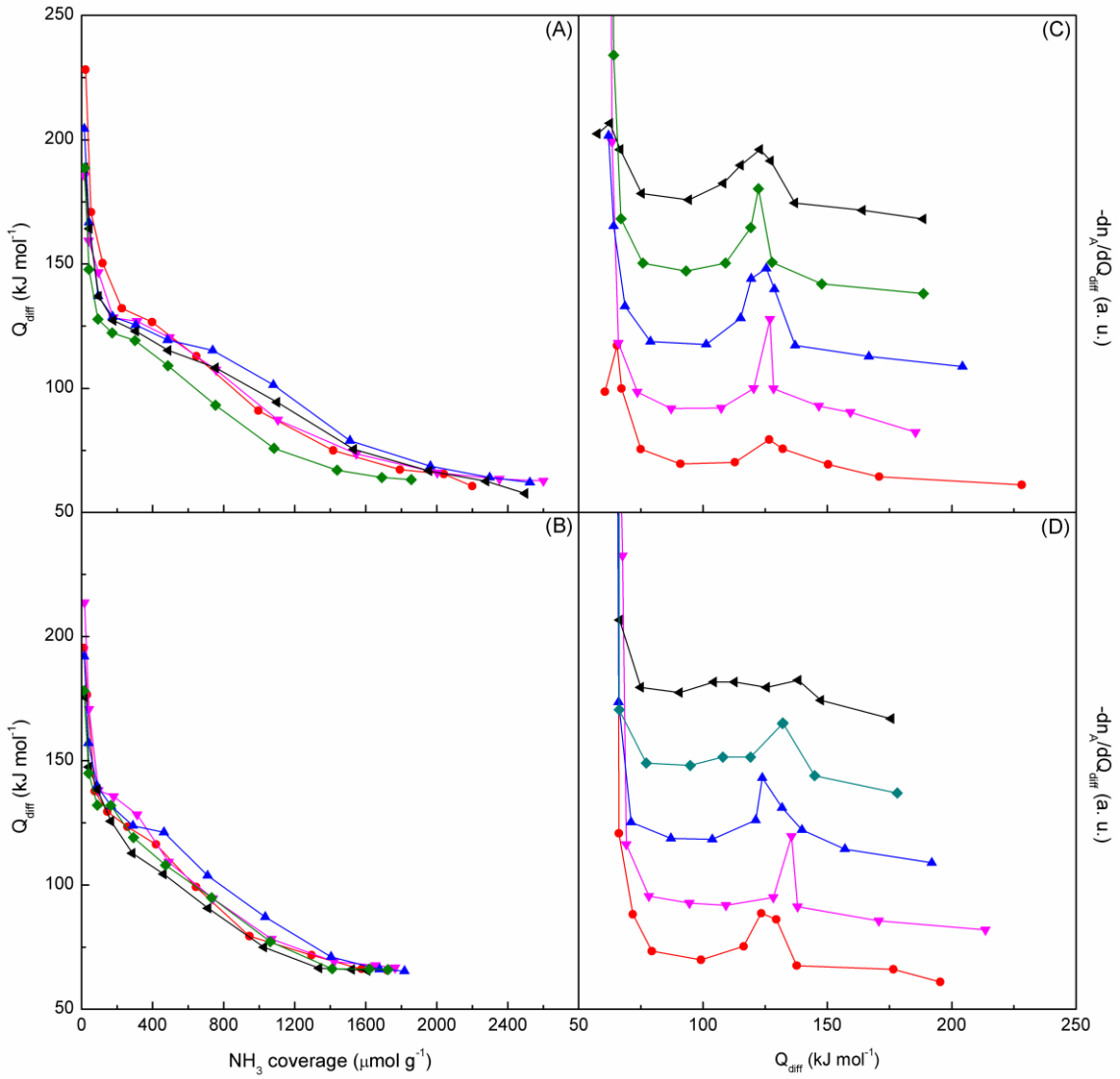

Fig. 4 Differential heats of adsorption vs. NH_3 coverage and acid sites strength distribution curves for the mono- and bimetallic catalysts based in HUSY (A, C) and HZSM5 (B, D). Curves of the parent zeolites (ZEO) are also reported. Symbols: (●) parent support; (▼) Pd-ZEO; (▲) Cu-ZEO; (◄) PdCu-ZEO and (◆) CuPd-ZEO.

The presence of different sets of sites, each set being homogeneous as to strength is revealed for each sample by the presence of peaks in its spectrum. As expected, for the present catalysts based in HUSY, a peak is observable in the Q_{diff} region between 110 and 150 kJ mol^{-1} (Fig. 4C), whose maximum is centered at about 125 kJ mol^{-1}.

The calorimetric curves of the parent HZSM5 and of the corresponding mono- and bimetallic catalysts are reported in Fig. 4B. Similar to the case of the catalysts based in HUSY, such samples exhibit high initial Q_{diff} values, in the range 175-215 kJ mol^{-1}. A quite rapid decrease in Q_{diff} as the coverage increases is observed. However, except for the PdCu-HZSM5, that shows a complete heterogeneity of the surface (its Q_{diff} profile continuously decreases with the ammonia uptake), a step is clearly visible for all the other samples between 115 and 135 kJ mol^{-1}, indicating the existence of a family of energetically homogeneous acid sites, as confirmed by the presence of a peak in the site energy distribution plots (Fig. 4D).

By disregarding the sites responsible for non-specific adsorption (i.e. with adsorption heats lower than the cut-off value), the acid sites strength distribution was evaluated by roughly ranking the sites as strong ($n_{A,s}$, $Q_{diff} \geq 150$ kJ mol^{-1}), medium ($n_{A,m}$, $100 \leq Q_{diff} < 150$ kJ mol^{-1}), and weak ($n_{A,w}$, $60 \leq Q_{diff} < 100$ kJ mol^{-1}) ones. The results are summarized in Table 5, where the concentration of the acid sites able to irreversibly adsorb NH_3 ($n_{A,irr}$) is also reported.

Table 5. Acid surface properties of the catalysts determined by adsorption microcalorimetry of NH_3.

Samples	$n_{A,w}$[a] (μmol/g)	$n_{A,m}$[b] (μmol/g)	$n_{A,s}$[c] (μmol/g)	$n_{A,irr}$[d] (μmol/g)
HUSY	1351	730	120	797
Pd-HUSY	1717	803	80	874
Cu-HUSY	1420	1034	71	1065
PdCu-HUSY	1438	887	72	1001
CuPd-HUSY	1218	598	40	626
HZSM5	1088	574	60	585
Pd-HZSM5	1116	571	77	588

Cu-HZSM5	1035	726	56	711
PdCu-HZSM5	1070	500	39	563
CuPd-HZSM5	1095	595	35	608

[a]weak acid sites ($60 \leq Q_{diff} < 100$ kJ mol^{-1}).
[b]medium acid sites ($100 \leq Q_{diff} < 150$ kJ mol^{-1}).
[c]strong acid sites ($Q_{diff} \geq 150$ kJ mol^{-1}).
[d]sites on which NH_3 is irreversibly adsorbed.

Compared to the parent HUSY, the Pd-HUSY and Cu-HUSY catalysts show a lower amount of strong acid sites, which is, however, accompanied by a noticeable increase in the $n_{A,w}$, $n_{A,m}$, and $n_{A,irr}$ number, especially in the case of Cu-HUSY. The addition of the second metal further modifies the acid surface properties of the monometallic samples. In comparison with the corresponding Cu-HUSY and Pd-HUSY catalysts, a general decrease in the acid sites concentration is observed, in fact, for PdCu-HUSY and CuPd-HUSY, the acidity of the latter being the lowest of the whole series of HUSY catalysts. By ranking the catalysts based on the irreversibly NH_3-adsorbing sites, the surface acidity is in the order: Cu-HUSY > PdCu-HUSY > Pd-HUSY > HUSY > CuPd-HUSY.

In the case of the catalysts based on HZSM5, the addition of a single metal component still seems to enhance the acidity compared to the parent zeolite; however, acid sites of different strength are affected by the introduction of Pd or Cu. In fact, while Pd addition increases the number of $n_{A,s}$ and $n_{A,w}$ sites, leaving that of $n_{A,m}$ and $n_{A,irr}$ almost unaltered, the presence of Cu results in a higher concentration of both $n_{A,m}$ and $n_{A,irr}$, with a concomitant slight decrease in the strong and weak acid sites amounts. With regard to the bimetallic samples, it can be noted that the PdCu-HZSM5 sample is notably less acidic than Cu-HZSM5. By converse, the introduction of Cu in the Pd-HZSM5 catalyst manifestly lowers the number of strong acid sites but causes a slight increase in both $n_{A,m}$ and $n_{A,irr}$ concentrations. Considering the

values of $n_{A,irr}$, the surface acidity of the mono- and bimetallic HZSM5 samples are in the order: Cu-HZSM5 > CuPd-HZSM5 > Pd-HZSM5 > HZSM5 > PdCu-HZSM5. By comparing the two HUSY- and HZSM5-based catalytic series, it appears that, except for the CuPd-HUSY and CuPd-HZSM5 samples, whose acidity is only slightly different, both the mono- and bimetallic catalysts based on HUSY possess a higher concentration of surface acid sites, regardless of their strength.

3.2. Catalytic efficiency of metal-ZEO catalysts in SA ozonation

All the prepared metal-ZEO catalysts were evaluated in the catalytic ozonation of SA in an aqueous solution at room temperature. The SA-removal efficiency of the HZSM5-based catalysts was superior to that of the HUSY-based ones, suggesting that different properties, such as surface area, pore volume, acidic character, and surface chemical composition, can affect the catalytic performance in the SA ozonation reaction at room temperature.

HZSM5-based catalysts. Fig. 5 shows the evolution of salicylic acid degradation and of total organic carbon (TOC) removal along with reaction time in the presence of the HZSM5-based catalysts (Fig. 5A and 5B, respectively).

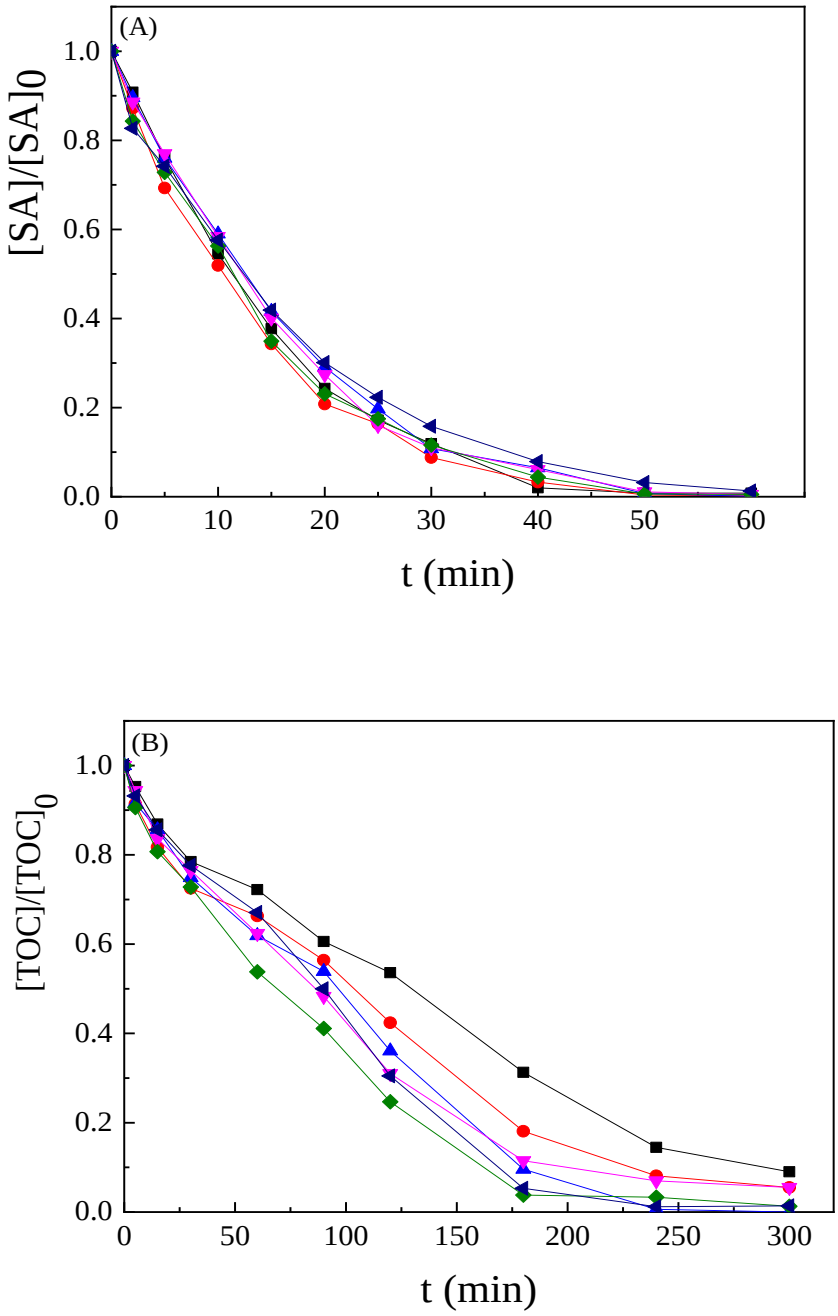

Fig. 5 Dimensionless salicylic acid (A) and TOC (B) concentration as a function of reaction time in the presence of HZSM5-based catalysts. Symbols: (■) single ozonation (O_3); (●) parent zeolite; (▼) Pd-HZSM5; (▲) Cu-HZSM5; (◄) PdCu-HZSM5 and (◆) CuPd-HZSM5.

It can be observed from Fig. 5A that both the homogeneous (not-catalyzed run labeled as single ozonation (O_3)) and the catalytic ozonation enable a fast decay of SA concentration, whose complete removal was attained in less than 60 min. This result is not unexpected since O_3 by itself can easily react with compounds containing either an activated aromatic ring or double bonds, degrading such pollutants by direct ozonation in solution. Similar behaviour has been reported in [41] for the removal of both nitrobenzene and benzoic acid in water using V-loaded ZSM-5 zeolites. However, single ozonation presents limitations in achieving high mineralization degrees [42,43], due to the formation of smaller intermediate molecules that can be effectively demolished by catalytic ozonation, while the homogeneous process is usually ineffective. Indeed, it is generally believed that the catalyst can improve the oxidation of the recalcitrant intermediates by three possible routes [44-47]: (i) chemisorption of ozone on the catalyst surface leading to the formation of active species, which react with non-chemisorbed organic molecule; (ii) chemisorption of the organic molecule (associative or dissociative) on the catalytic surface and its further reaction with gaseous or aqueous ozone; (iii) chemisorption of both ozone and organic molecules and the subsequent interaction between chemisorbed species. The relative extent to which the different mechanisms can occur depends on the differences in the catalyst properties, the properties of the target organic compounds, and the operating conditions.

In order to distinguish between single and catalytic ozonation in eliminating not only SA, but also the eventually formed recalcitrant intermediates, the TOC removal was also followed (Fig. 5B), and the obtained results clearly suggest that such intermediates are formed and that the presence of the catalyst is necessary to improve their mineralization. All the HZSM5-based catalysts show a better performance in

comparison with single ozonation. After 300 min, the mono- and bimetallic Cu-HZSM5 catalysts are able to completely degrade the organic matter, while in the case of HZSM5 and Pd-HZSM5, a small fraction of the total organic carbon (ca. 5%) is still present, which is however higher (9%) in the absence of the catalyst. By considering lower reaction times, greater differences are observed in the dimensionless TOC values, indicating different rates of mineralization, which after 120 min are in the order: O_3 < HZSM5 < Cu-HZSM5 < Pd-HZSM5 ≃ PdCu-HZSM5 < CuPd-HZSM5. Such result indicates that the addition of the metals improves TOC removal and that the bimetallic catalysts perform better than the monometallic ones. Interestingly, the best performance is shown by the CuPd-HZSM5 catalyst, which exhibits the highest Cu(0)/Cu(II) and Pd(0)/Pd(II) atomic ratios. These results show that the behaviour of the HZSM5-based catalysts depends on the physicochemical properties of the MFI structure.

HUSY-based catalysts. Unlike the HZSM5-based catalyst, for which single ozonation, the parent zeolite and its metal-based catalysts exhibit comparable SA removals (Fig. 5A) most of the HUSY-based catalysts have lower performance than single ozonation (Fig. 6A). SA removal efficiencies appear to be influenced by the physicochemical properties, the composition, and, for the bimetallic catalysts, the order of introduction of the metals during the synthesis. In particular, the worst behavior is shown by the PdCu-HUSY, for which, contrary to all the other catalysts, the complete removal of SA is not achieved even after 60 min of reaction. Both Pd-HUSY and CuPd-HUSY are able to completely eliminate SA within 40 min (the former showing a better performance in terms of degradation rate), whereas about

20% of the pollutant is still present at this reaction time in the presence of the parent HUSY and of Cu-HUSY.

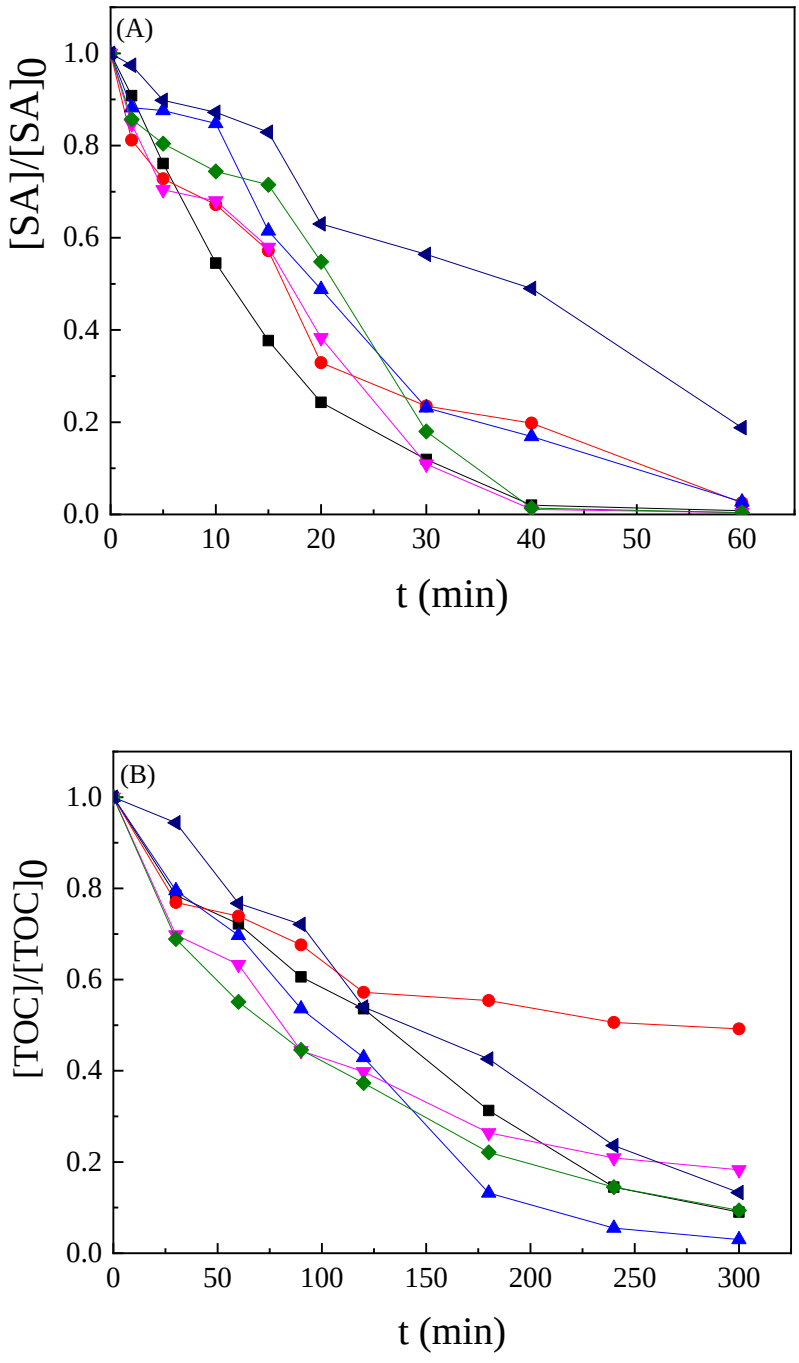

Fig. 6 Dimensionless salicylic acid (A) and TOC (B) concentration as a function of reaction time in the presence of HUSY-based catalysts. Symbols: (■) single

ozonation (O_3); (●) parent zeolite; (▼) Pd-HUSY; (▲) Cu-HUSY; (◄) PdCu-HUSY; (◆) CuPd-HUSY.

However, in the presence of the HUSY-based catalysts, better efficiency of the organic matter removal is generally observed (Fig. 6B): though HUSY presents a lower TOC removal than single ozonation, the introduction of the metal species into the zeolite structure leads to higher mineralization levels. Cu-HUSY shows the best performance, achieving nearly complete mineralization after 300 min of reaction. This result could be related to the high surface area and Cu content of this sample (cf. Tables 1 and 2). Peculiarly, as already observed in the case of the HZSM5-based catalysts, the CuPd-HUSY, which exhibits higher M(0)/M(II) ratios compared to PdCu-HUSY (Table 4), shows the best performance between the two bimetallic catalysts, suggesting that such parameter is important in favouring the complete mineralization process.

The different performance of the catalysts based on HZSM5 and HUSY can be related to their different textural properties, surface acidity and hydrophobicity, and chemical composition at the surface. Though catalytic ozonation is considered to be enhanced by an increase in surface area [48], the better performance showed by HZSM5 (with a lower surface area) in comparison with HUSY seems to suggest that the percentage of mesopores may also play a role. Indeed, the V_{meso} value of HZSM5 is higher than that of HUSY and accounts for 62% of the total volume (while is only 38% for HUSY). Moreover, the higher Si/Al ratio of HZSM5 and its lower concentration of acid sites (Table 5) also seem to favour SA degradation. Additionally, the excellent catalytic activity of the metal-containing HZSM5-based catalysts may be mainly attributed to the presence of different concentrations and

oxidation states of the metal species attached to the ion-exchange sites of the zeolite as displayed by the XPS results (Tables 3 and 4). Kim et al [18] show that the ozonation of toluene at room temperature using Ru-Mn supported on Y and ZSM5 zeolites as catalysts is influenced by the zeolite used as the support. Catalysts with strong acidic sites, such as the bimetallic catalysts based in ZSM5, had significantly higher toluene removal efficiencies than the bimetallic Ru-MnY catalysts, due to the differences in the specific surface area, pore volume, number of active sites, and surface acidity. In addition, the chemical surface composition was an important aspect for determining the catalytic activity [18].

Several organic intermediates can be formed during SA degradation [3], as confirmed by the differences in the trends of SA concentration and of the total organic carbon as a function of time (Fig. 5 and 6), one of them being oxalic acid (Oxl). The evolution of such compound as a function of time was then monitored up to 300 min during the SA ozonation reaction and the results are reported in Fig. 7.

The HZSM5-based catalysts still show better performance than the HUSY-based catalysts, confirming that the catalytic activity strongly depends on the zeolite structure used as the support.

Concerning the HZSM5-based catalysts, for most cases the highest Oxl concentration is achieved after 120 min, with values in the range 0.230-0.335 mM, which indicates that Oxl is one of the major by-products of SA degradation, whose amount increases in the order $O_3 \simeq$ HZSM5 > CuPd-HZSM5 > Pd-HZSM5. Oxalic acid is instead detected in much lower amounts on Cu-HZSM5 and PdCu-HZSM5, with maxima (0.077 and 0.056 mM, respectively) observed after 45 min of reaction.

In the case of HUSY-based catalysts, small amounts of Oxl are formed during catalytic ozonation, and no oxalic acid was released after 180 min of reaction. This

result is not surprising, since catalytic ozonation in the presence of the HUSY-based catalysts led to worse results in terms of TOC removal; therefore, a different reaction pathway seems to be occurring with the formation of high amounts of recalcitrant intermediates, and the formation of oxalic acid, as a final oxidation organic byproduct is not favored.

To shed light on the role of the catalyst, degradation of Oxl was investigated in the same operative conditions used for SA ozonation conditions in the presence of HZSM5-based catalysts, and the results are presented in Fig. 8.

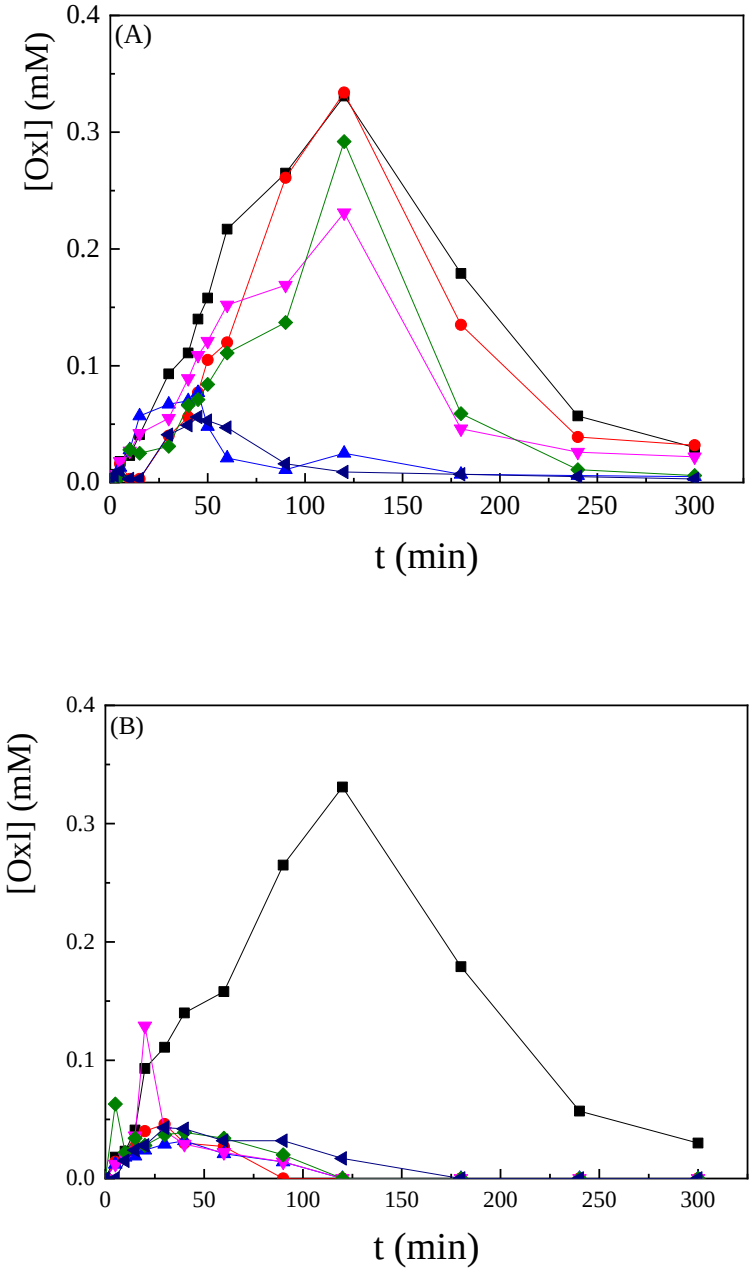

Fig. 7 Evolution of oxalic acid (Oxl) concentration along with the reaction time during SA degradation in the presence of catalysts based on HZSM5 (A) and HUSY (B). Symbols: (■) single ozonation (O_3); (●) parent zeolite; (▼) Pd-ZEO; (▲) Cu-ZEO; (◄) PdCu-ZEO and (◆) CuPd-ZEO.

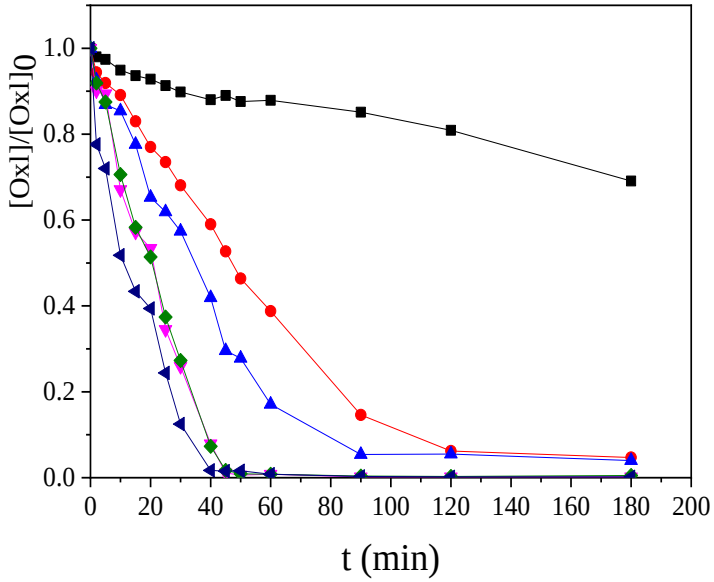

Fig. 8 Dimensionless oxalic acid (Oxl) concentration as a function of reaction time in the presence of catalysts based on HZSM5. Symbols: (■) single ozonation (O_3); (●) parent zeolite; (▼), Pd-HZSM5; (▲) Cu-HZSM5; (◄) PdCu-HZSM5 and (◆) CuPd-HZSM5.

The results clearly show the beneficial effect of the catalyst on the degradation of Oxl, also confirming the general improvement in activity in the presence of bimetallic catalysts and suggesting the existence of a synergistic effect. After 50 min, Oxl is completely removed in the presence of Pd-HZSM5, CuPd-HZSM5, and PdCu-HZSM5, while Cu-HZSM5, HZSM5, and O_3 are able to mineralize 72, 54, and 12% of the initial Oxl amount, respectively. Differences in the rate of oxalic acid degradation can be emphasized at lower reaction times: after 25 min, the percentages of removal are in the order: O_3 (9%) < HZSM5 (26%) < Cu-HZSM5 (38%) < Pd-HZSM5 (63%) ≃ CuPd-HZSM5 (65%) < PdCu-HZSM5 (76%).

Degradation of Oxl in the presence of the HZSM5-based catalysts confirms the better performance of these materials for the ozonation process, with a total conversion being achieved in a short reaction time.

In the degradation of SA using mesoporous Fe-Cu@SiO_2 core-shell catalyst, several molecules were identified as ozonation products, as catechol, 2,3-dihydroxybenzoic acid and 2,5-dihydroxybenzoic acid (2,5-DHBA) followed by the opening of the rings to form carboxylic acids, as Oxl, and mineralization [49,50]. In the light of the results, it can be reasonably supposed that SA molecules adsorb on the ZEO-based zeolites that produce several intermediates as aromatic by-products until carboxylic acids and total mineralization was obtained with HZSM5-based catalysts (Fig. 9).

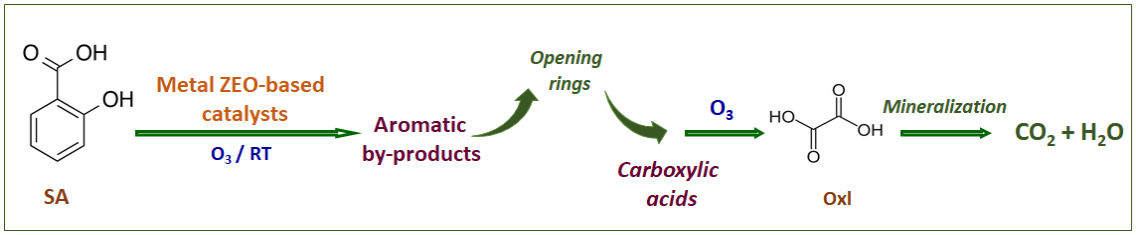

Fig. 9 Proposed degradation pathway of salicylic acid using ZEO-based catalyst by ozonation.

A long-term experiment was carried out with the best-performing catalysts (CuPd-ZEO) in order to verify their stability and reusability after five reaction cycles, each one lasting 5 h (Fig. 10). No leaching of Pd or Cu was detected (within the experimental error) at the end of the reaction test, revealing that the catalysts are stable.

Both bimetallic catalysts remain highly active after the fifth reaction cycle, although a small decrease in the SA removal percentage can be noted for the CuPd-HZSM5 catalyst. In addition, also the percentage of TOC removal remains almost constant

during the stability test, except for the slight decrease observed for the CuPd-HUSY catalyst after the fifth cycle.

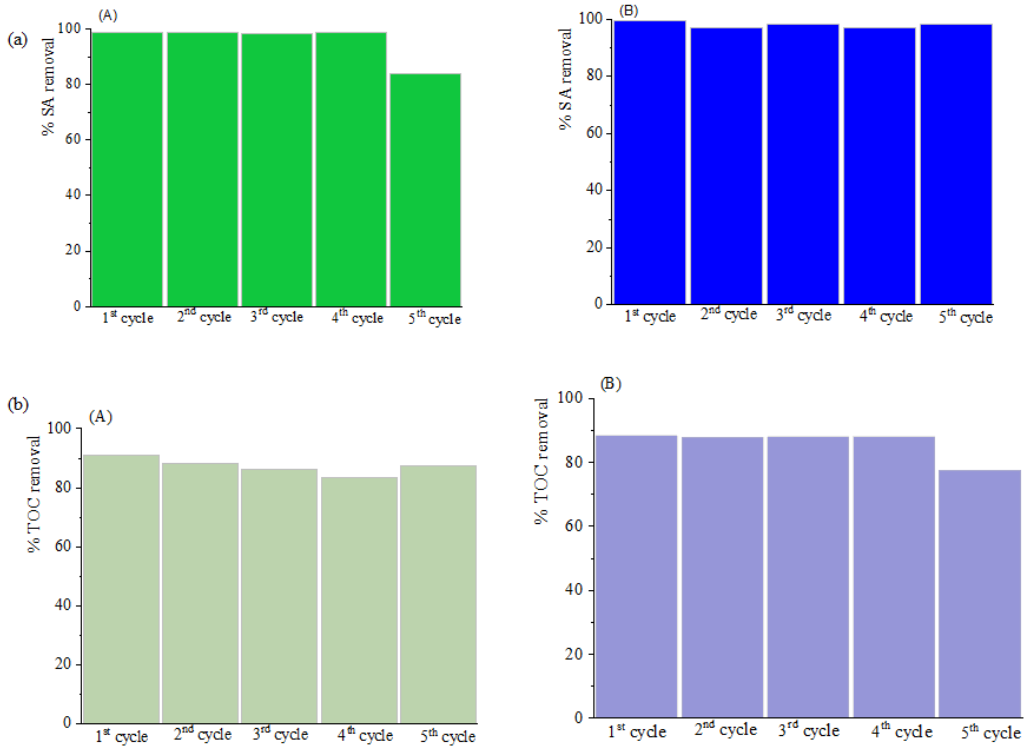

Fig. 10 (a) SA removal efficiency and (b) TOC removal efficiency along five cycles, after 300 min of reaction, during the mineralization of SA in the presence of CuPd-ZEO catalysts based on HZSM5 (A) and HUSY (B).

At the end of the reusability tests, the CuPd-ZEO catalysts were characterized by SEM/EDX in order to check for any changes in the zeolite morphology. SEM micrographs demonstrate that the typical morphology of the parent zeolites was preserved (Fig. 11).

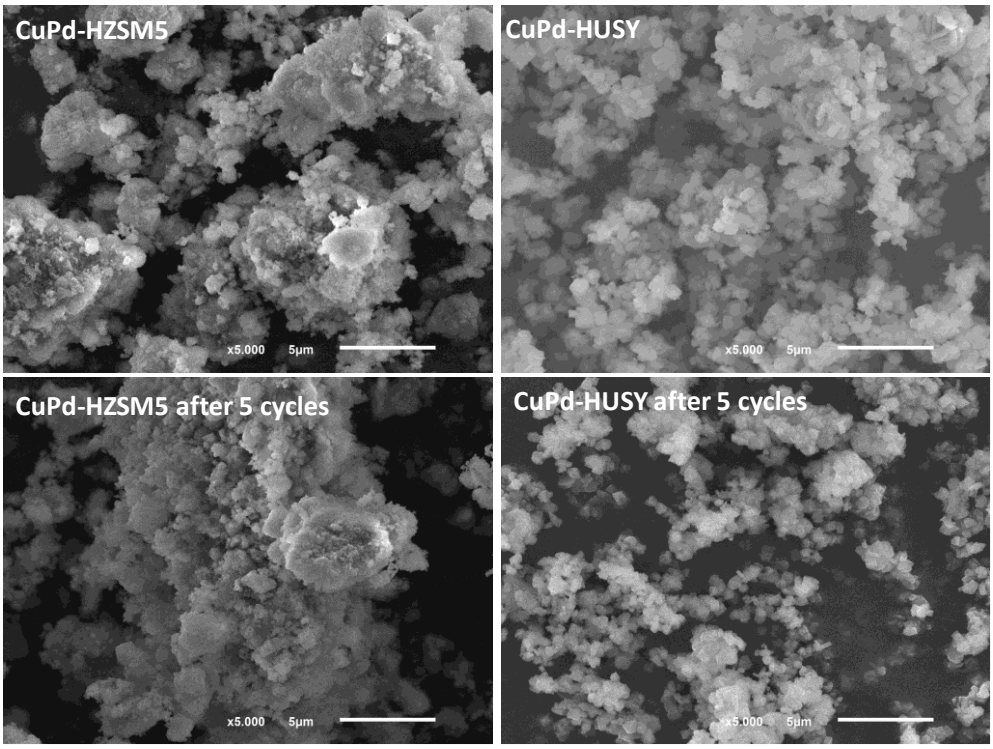

Fig. 11 SEM images of CuPd-HZSM5 and CuPd-HUSY before and after five reaction cycles.

Moreover, EDX analysis showed that the Pd (1.6 and 1.3 wt% for CuPd-HUSY and CuPd-HZSM5, respectively) and Cu amounts (0.5 and 0.7 wt% for CuPd-HUSY and CuPd-HZSM5, respectively) are comparable to those determined on the fresh samples (Table 2), confirming the absence of leaching phenomena. These results clearly show that the catalysts are very stable.

4 CONCLUSIONS

Metal-zeolite catalysts were successfully prepared by adding palladium and/or copper over HUSY or HZSM5 through the ion-exchange method. The obtained samples were used as catalysts in the ozonation reaction of salicylic acid (SA) and proved to be efficient for degrade very stable molecules in the aquatic environment, as SA, since the presence of this pollutant in effluents has been related to toxic effects

in aquatic organisms, including oxidative stress. The catalytic performance was found to depend on the zeolite structure used. While the parent HZSM5 was already a suitable ozonation catalyst for SA degradation, the combination of HUSY with O_3 was not advantageous. The introduction into the zeolite structures of Cu and Pd as the only metal component or in combination to obtain the bimetallic catalysts enhanced the catalytic activity, especially in terms of mineralization degree, but distinct behaviors were evidenced between the two investigated ZEO-based catalysts. The catalytic ability is dependent on the specific surface area, pore volume, number of active sites, and surface acidity of the different zeolite used as supports. Moreover, the catalyst chemical composition, such as Pd/Cu ratios, were found to be important factors for determining the catalytic activity of the catalysts. The CuPd-ZEO catalysts presented the best results and the stability tests showed that they could be used after five cycles without significant loss of activity.

Conflicts of interest

There are no conflicts of interest to declare

ACKNOWLEDGEMENTS

This work has been developed under the scope of the projects: BioTecNorte (operation NORTE-01-0145-FEDER-000004) and "AIProcMat@N2020-Advanced Industrial Processes and Materials for a Sustainable Northern Region of Portugal 2020", NORTE-01-0145-FEDER-000006, supported by the Northern Portugal Regional Operational Programme (NORTE 2020), under the Portugal 2020 Partnership Agreement, through the European Regional Development Fund (ERDF). This work also has been funded by national funds (FCT, Foundation for Science and

Technology, Portugal), through the projects: PTDC/AAGTEC/5269/2014, Centre of Chemistry (UID/QUI/00686/2013 and UID/QUI/0686/2016) and LSRE/LCM (UIDB/50020/2020 and UIDP/50020/2020). O.S.G.P.S. acknowledges FCT funding under the Scientific Employment Stimulus - Institutional Call CEECINST/00049/2018. C.A.O. acknowledges FCT funding under DL57/2016 Transitory Norm Programme.

5 REFERENCES

[1] R. Costa, R.M. Quinta-Ferreira, R.C. Martins, Application of ozonation for pharmaceuticals and personal care products removal from water, *Sci. Total Environ.,* 2017, *586*, 265-283.

[2] D. Li, J. Qu, The progress of catalytic technologies in water purification: a review, *J. Environ. Sci.,* 2009, *21*, 713-719.

[3] R. Hu, L. Zhang, J. Hu, Study on the kinetics and transformation products of salicylic acid in water via ozonation, *Chemosphere*, 2016, *153*, 394-404.

[4] K. Zitta, P. Meybohm, B. Bein, Y. Huang, C. Heinrich, J. Scholz, M. Steinfath, M. Albrecht, Salicylic acid induces apoptosis in colon carcinoma cells grown in-vitro: influence of oxygen and salicylic acid concentration, *Exp. Cell Res.* 2012, *318*, 828-834.

[5] X.L. Tan, K.M.R. Lombardo, W.R. Bamlet, A.L. Oberg, D.P. Robinson, K.E. Anderson, G.M. Petersen, Aspirin, nonsteroidal anti-inflammatory drugs, acetaminophen, and pancreatic cancer risk: a clinic-based case-control study, *Cancer Prev. Res. (Phila.),* 2011, *4*, 1835-1841.

[6] J. Wang, Z. Bai, Fe-based catalysts for heterogeneous catalytic ozonation of emerging contaminants in water and wastewater, *Chem. Eng. J.,* 2017, *312*, 79-98.

[7] A.G. Gonçalves, J.J.M. Órfão, M.F.R. Pereira, Catalytic ozonation of sulphamethoxazole in the presence of carbon materials: catalytic performance and reaction pathways, *J. Hazard. Mater.,* 2012*, 239-240*,167-174.

[8] F.J. Beltrán, P. Pocostales, P. Alvarez, A. Oropesa, Diclofenac removal from water with ozone and activated carbon, *J. Hazard. Mater.,* 2009, *163*, 768–776.

[9] M. Sánchez-Polo, J. Rivera-Utrilla, G. Prados-Joya, M.A. Ferro-García, I. Bautista-Toledo, Removal of pharmaceutical compounds, nitroimidazoles, from waters by using the ozone/carbon system, *Water Res.,* 2008, *42*, 4163–4171.

[10] A.G. Gonçalves, J.J.M. Órfão, M.F.R. Pereira, Ozonation of bezafibrate promoted by carbon materials, *Appl. Catal. B: Environ.,* 2013, *140–141*, 82–91.

[11] C.M.A.S. Freitas, O.S.G.P. Soares, J.J.M. Órfão, A.M. Fonseca, M.F.R. Pereira, I.C. Neves, Highly efficient reduction of bromate to bromide over mono and bimetallic ZSM5 catalysts, *Green Chem.,* 2015, *17*, 4247-4254.

[12] O.S.G.P. Soares, C.M.A.S. Freitas, A.M. Fonseca, J.J.M. Órfão, M.F.R. Pereira, I.C. Neves, Bromate reduction in water promoted by metal catalysts prepared over faujasite zeolite, *Chem. Eng. J.,* 2016, *291*, 199-205.

[13] O.S.G.P. Soares, L. Marques, C.M.A.S. Freitas, A.M. Fonseca, P. Parpot, J.J.M. Órfão, M.F.R. Pereira, I.C. Neves, Mono and bimetallic NaY catalysts with high performance in nitrate reduction in water, *Chem. Eng. J.,* 2015, *281*, 411-417.

[14] O.S.G.P. Soares, A.M. Fonseca, P. Parpot, J.J.M. Órfão, M.F.R. Pereira, I.C. Neves, Oxidation of volatile organic compounds by highly efficient metal zeolite catalysts, *ChemCatChem,* 2018*, 10*, 3754-3760.

[15] M. Ziółek, J. Nawrocki, B. Kasprzyk-Hordern, Catalytic ozonation and methods of enhancing molecular ozone reactions in water treatment, *Appl. Catal. B:Environ.,* 2003, *46*, 639-669.

[16] Y. Shu, M. He, J. Ji, H. Huang, S. Liu, D.Y.C. Leung, Synergetic degradation of VOCs by vacuum ultraviolet photolysis and catalytic ozonation over Mn-xCe/ZSM-5. *J. Hazard. Mater.,* 2019, *364*, 770–779.

[17] S.K.P. Veerapandian, N.D. Geyter, J.-M. Giraudon, J.-F. Lamonier, R. Morent, The use of zeolites for VOCs abatement by combining non-thermal plasma, adsorption, and /or catalysis: a review, *Catalysts*, 2019, *9*, 98.

[18] J. Kim, E.E. Kwon, J.E. Lee, S.-Ho Jang, J.-Ki Jeon, J. Song, Y.-K. Park, Effect of zeolite acidity and structure on ozone oxidation of toluene using Ru-Mn loaded zeolites at ambient temperature*, J. Hazard. Mater.,* 2021*, 403*, 123934.

[19] A. Ikhlaq, S. Waheed, K.S. Joya, M. Kazmi, Catalytic ozonation of paracetamol on zeolite A: Non-radical mechanism, *Catal. Commun.,* 2018*, 112*, 15-20.

[20] A. Ikhlaq, D.R. Brown, B. Kasprzyk-Hordern, Catalytic ozonation for the removal of organic contaminants in water on ZSM-5 zeolites*, Appl. Catal. B: Environ.,* 2014*, 154*, 110-122.

[21] J. Rouquerol, P. Llewellyn, F. Rouquerol, "Is the BET equation applicable to microporous adsorbents?", in: Characterization of porous solids VII. P. Llewellyn, F. Rodriguez-Reinoso, J. Rouquerol, and N. Seaton (Eds*): Studies in Surface Science and Catalysis,* 2007, *160*, 49-56.

[22] S.M. Seo, W.T. Lim, K. Seff, Crystallographic Verification that Copper(II) Coordinates to Four of the Oxygen Atoms of Zeolite 6-Rings. Two Single-Crystal Structures of Fully Dehydrated, Largely Cu2+-Exchanged Zeolite Y (FAU, Si/Al = 1.56), *J. Phys. Chem. C,* 2012*, 116*, 963–974.

[23] Y.M. Lee, S.J. Choi, Y. Kim, K. Seff, Crystal Structure of an Ethylene Sorption Complex of Fully Vacuum-Dehydrated Fully Ag+-Exchanged Zeolite X (FAU).

Silver Atoms Have Reduced Ethylene To Give CH22- Carbanions at Framework Oxide Vacancies, *J. Phys. Chem. B* 2005*, 109*, 20137-20144.

[24] B. Gu, L. Wang, S. Wang, D. Zhao, V.H. Rotberg, R.C. Ewing, The effect of H+ irradiation on the Cs-ion-exchange capacity of zeolite-NaY, *J. Mater. Chem.,* 2000*, 10,* 2610-2616.

[25] J.F. Moulder, Handbook of X-ray Photoelectron Spectroscopy: A Reference Book of Standard Spectra for Identification and Interpretation of XPS Data, ed. Jill Chastain, Physical Electronics Division, Perkin-Elmer Corporation, 1992.

[26] G. Deroubaix, P. Marcus, X-ray photoelectron spectroscopy analysis of copper and zinc oxides and sulphides, *Surf. Interface Anal.* 1992, *18*, 39-46.

[27] A.V. Naumkin, A. Kraut-Vass, S.W. Gaarenstroom, Powell, C.J. NIST Standard Reference Database 20, Version 4.1 (web version) (http:/srdata.nist.gov/xps/), 2012.

[28] M.C. Biesinger, L.W.M. Lau, A.R. Gerson, R.St.C. Smart, Resolving surface chemical states in XPS analysis of first row transition metals, oxides and hydroxides: Cr, Mn, Fe, Co and Ni, *Appl. Surf. Sci.,* 2010, *257*, 887-898.

[29] M.C. Militello, S.J. Simko, Elemental palladium by XPS, *Surf. Sci. Spectra,* 1994*, 3*, 387-394.

[30] K.R. Priolkar, P. Bera, P.R. Sarode, M.S. Hegde, S. Emura, R. Kumashiro, N.P. Lalla, Formation of Ce1-xPdxO2-δ Solid Solution in Combustion-Synthesized Pd/CeO2 Catalyst: XRD, XPS, and EXAFS Investigation, *Chem. Mater.,* 2002*, 14*, 2120-2128;

[31] W. Zhang, H. Huang, F. Li, K. Deng, X. Wang, Palladium nanoparticles supported on graphitic carbon nitride-modified reduced graphene oxide as highly efficient catalysts for formic acid and methanol electrooxidation, *J. Mater. Chem. A, 2* (2014) 19084-19094.

[32] M. Peuckert, XPS study on surface and bulk palladium oxide, its thermal stability, and a comparison with other noble metal oxides, *J. Phys. Chem.,* 1985*, 89(12)*, 2481-2486.

[33] D. Gašparovičová, M. Králik, M. Hronec, Z. Vallušová, H. Vinek, B. Corain, Supported Pd–Cu catalysts in the water phase reduction of nitrates: Functional resin versus alumina, *J. Mol. Catal. A: Chem.,* 2007*, 264*, 93-102.

[34] C.M. Mendez, H. Olivero, D.E. Damiani, M.A. Volpe, On the role of Pd β-hydride in the reduction of nitrate over Pd based catalyst*, Appl. Catal. B: Environ.,* 2008*, 84*, 156-161.

[35] S.S. Priya, P. Bhanuchander, V.P. Kumar, S.K. Bhargava, K.V.R. Chary, Activity and selectivity of platinum–copper bimetallic catalysts supported on mordenite for glycerol hydrogenolysis to 1, 3-propanediol, *Ind. Eng. Chem. Res.,* 2016*, 55*, 4461-4472.

[36] J. Batista, A. Pintar, D. Mandrino, M. Jenko, V. Martin, XPS and TPR examinations of γ-alumina-supported Pd-Cu catalysts, *Appl. Catal. A-Gen.,* 2001, *206,* 113-124.

[37] J. Zheng, M. Guo, C. Song, Characterization of Pd catalysts supported on USY zeolites with different SiO2/Al2O3 ratios for the hydrogenation of naphthalene in the presence of benzothiophene, *Fuel Process. Technol.* 2008*, 89*, 467-474.

[38] S. Echeandia, B. Pawelec, V.L. Barrio, P.L. Arias, J.F. Cambra, C.V. Loricera, J.L.G. Fierro, Enhancement of phenol hydrodeoxygenation over Pd catalysts supported on mixed HY zeolite and Al2O3. An approach to O-removal from bio-oils, *Fuel,* 2014*, 117*, 1061-1073.

[39] Z. Zhang, L. Xu, Z. Wang, Y. Xu, Y. Chen, Pd/Hβ-zeolite catalysts for catalytic combustion of toluene: Effect of SiO2/Al2O3 ratio, *J. Nat. Gas Chem.,* 2010*, 19*, 417-421.

[40] D.M. Ruthven, Principles of adsorption & adsorption processes, New York, Wiley, 1984.

[41] Y. Xu, Q. Wang, B.A. Yoza, Q.X. Li, Y. Kou, Y. Tang, H. Ye, Y. Li, C. Chen, Catalytic Ozonation of Recalcitrant Organic Chemicals in Water Using Vanadium Oxides Loaded ZSM-5 Zeolites, *Front. Chem.* 2019*, 7*, 384. (doi: 10.3389/fchem.2019.00384).

[42] C.A. Orge, J.L. Faria, M.F.R. Pereira, Photocatalytic ozonation of aniline with TiO2-carbon composite materials*, J. Environ. Manage,* 2017*, 195*, 208-215.

[43] C.A. Orge, M.F.R. Pereira, J.L. Faria, Photocatalytic-assisted ozone degradation of metolachlor aqueous solution, *Chem. Eng. J.,* 2017*, 318*, 247-253.

[44] B. Kasprzyk-Hordern, M. Ziółek, J. Nawrocki, Catalytic ozonation and methods of enhancing molecular ozone reactions in water treatment, *Appl. Catal. B: Environ.,* 2003*, 46*, 639 669.

[45] J. Nawrocki, Catalytic ozonation in water: Controversies and questions. Discussion paper, *Appl. Catal. B: Environ.,* 2013*, 142-143*, 465-471.

[46] J.L. Rodríguez, I. Fuentes, C.M. Aguilar, M.A. Valenzuela, T. Poznyak, I. Chairez, Catalytic Ozonation as a Promising Technology for Application in Water Treatment: Advantages and Constraints, in Ozone in Nature and Practice, Ch. 2, pp. 17-36, IntechOpen 2018, http://dx.doi.org/10.5772/intechopen.76228.

[47] J. Gomes, R. Costa, R.M. Quinta-Ferreira, R.C. Martins, Application of ozonation for pharmaceuticals and personal care products removal from water, *Science of the Total Environment,* 2017*, 586*, 265-283.

[48] O.S.G.P. Soares, A.G. Gonçalves, J.J. Delgado, J.J.M. Órfão, M.F.R. Pereira, Modification of carbon nanotubes by ball-milling to be used as ozonation catalysts, *Catal. Today,* 2015*, 249,* 199-203.

[49] W. Chen, Y. Bao, X. Li, J. Huang, Y. Tang, L. Li, Mineralization of salicylic acid via catalytic ozonation with Fe-Cu@SiO2 core-shell catalyst: A two-stage first order reaction, *Chemosphere,* 2019, *235*, 470-480.

[50] R. Hu, L. Zhang, J. Hu, Study on the kinetics and transformation products of salicylic acid in water via ozonation, *Chemosphere* 2016*, 153,* 394-404.